Vol. 87 No. 5 pp. 1355–1369 ACTA GEOLOGICA SINICA (English Edition) Oct. 2013

Isotopic Compositions of Sulfur in the Jinshachang Lead–Zinc Deposit, Yunnan, China, and its Implication on the Formation of Sulfur-Bearing Minerals

BAI Junhao[1,2,3], HUANG Zhilong[1,*], ZHU Dan[1], YAN Zaifei[1] and ZHOU Jiaxi[1]

1 *State Key Laboratory of Ore Deposit Geochemistry, Institute of Geochemistry, Chinese Academy of Sciences, Guiyang 550002, China*

2 *Henan Institute of Geological Survey, Zhengzhou 450001,China*

3 *Graduate University of Chinese Academy of Sciences, Beijing 100049, China*

Abstract: The Jinshachang lead–zinc deposit is mainly hosted in the Upper Neoproterozoic carbonate rocks of the Dengying Group and located in the Sichuan–Yunnan–Guizhou (SYG) Pb–Zn–Ag multi-metal mineralization area in China. Sulfides minerals including sphalerite, galena and pyrite postdate or coprecipitate with gangue mainly consisting of fluorite, quartz, and barite, making this deposit distinct from most lead–zinc deposits in the SYG. This deposit is controlled by tectonic structures, and most mineralization is located along or near faults zones. Emeishan basalts near the ore district might have contributed to the formation of orebodies. The δ^{34}S values of sphalerite, galena, pyrite and barite were estimated to be 3.6‰–13.4‰, 3.7‰–9.0‰, −6.4‰ to 29.2‰ and 32.1‰–34.7‰, respectively. In view of the similar δ^{34}S values of barite and sulfates being from the Cambrian strata, the sulfur of barite was likely derived from the Cambrian strata. The homogenization temperatures ($T \approx$ 134–383°C) of fluid inclusions were not suitable for reducing bacteria, therefore, the bacterial sulfate reduction could not have been an efficient path to generate reduced sulfur in this district. Although thermochemical sulfate reduction process had contributed to the production of reduced sulfur, it was not the main mechanism. Considering other aspects, it can be suggested that sulfur of sulfides should have been derived from magmatic activities. The δ^{34}S values of sphalerite were found to be higher than those of coexisting galena. The equilibrium temperatures calculated by using the sulfur isotopic composition of mineral pairs matched well with the homogenization temperature of fluid inclusions, suggesting that the sulfur isotopic composition in ore-forming fluids had reached a partial equilibrium.

Key words: sulfur isotopic composition, thermochemical sulfate reduction, homogenization temperature, equilibrium temperature, Jinshachang lead–zinc deposit

1 Introduction

The Sichuan–Yunnan–Guizhou (SYG) Pb–Zn–Ag multimetal mineralization area, located in the Permian Emeishan Large Igneous Province (ELIP) in the southwest of China, is the major source base of Pb, Zn and Ag and has more than 400 lead–zinc deposits and ore spots. In the ELIP, voluminous basalts were responsible for the formation of various types of deposits and made them more complicated (Hu et al., 2005). It has already been proved that the formation of the well-studied Huize lead–zinc deposit, the largest one in the SYG area, is partly related to eruption of the Emeishan basalts (Huang et al., 2003; Li et al., 2007). However, other large lead–zinc deposits in the SYG, such as the Jinshachang and the Maozu lead–zinc deposits, have not been paid enough attention recently, and their ore genesis is still controversial (Liu and Lin, 1999). The Jinshachang carbonate-hosted lead–zinc deposit, located in the northeast of Yunnan province, is surrounded by Emeishan basalts in the northwest of the SYG area. Liu and Lin (1999) and Zhang (1988) demonstrated that the Jinshachang deposit was a sedimentary-transformed epigenetic deposit controlled by the thermal events of Emeishan basalts. Liu (1989) had shown that this deposit

* Corresponding author. E-mail: huangzhilong@vip.gyig.ac.cn

was of MVT type and the sulfides minerals were formed by the thermochemical reduction of sulfates minerals present in the upper or lower strata. Although many studies had been carried out (Liu and Lin, 1999; Liu, 1989; Tu, 1984), the source of sulfur and mechanisms for the precipitation of ore minerals were poorly constrained.

In some deposits, such as Huize (Huang et al., 2010; Li et al., 2006) and Maozu (Liu and Lin, 1999), the major gangue mineral is calcite. However, the Jinshachang deposit is characterized by a special association between sulfides and sulfate minerals, which make it much more distinctive from other lead–zinc deposits in the SYG area and help us obtain crucial information on the source of sulfur and the physiochemical characteristics of ore-forming fluids (Arnold and Sheppard, 1981; Heyl et al., 1974; Ohmoto, 1972; Seal, 2006). Therefore, systemic studies on detailed ore geology, stable isotope, fluid inclusion, and other geochemical fields in this deposit are helpful not only in tracing the migration of ore-forming elements but also in finding out the relationship between the Emeishan basalts and lead–zinc mineralization in the SYG area.

Studies on sulfur isotope have helped understand the precipitation processes of ore minerals (Ohmoto, 1972; Seal, 2006), hence, such studies have popularly been used to investigate the origin of the deposits. Although sulfur isotopic components of sulfides minerals in the Jinshachang lead–zinc deposit have been reported, the genesis of reduced sulfur is still controversial. On the basis of the sulfur isotopic components of sulfides minerals, Tu (1984) proposed that the deep seated sulfur was incorporated into ore-forming fluids, but the sulfur isotopic components of sulfate were not discussed in his study. Liu (1989) showed that the sulfur of sulfides were derived from marine sulfates during the same period when thermochemical sulfate reduction (TSR) took place, However, he did not consider the sulfur isotopic fractionation between sulfides and sulfates. In this study, systemic sulfur isotopic compositions of sulfides and barite from the Jinshachang lead–zinc deposit district were analyzed, to discuss 1) the precipitation mechanism of sulfides and barite 2) the isotopic equilibrium between galena and sphalerite, and 3) the relationship between sources of sulfur (sulfide and sulfate) and magmatic activities.

2 Geological Setting

2.1 Regional geology

The South China Block consists of two major Precambrian blocks: the Yangtze Block in the northwest and the Cathaysia Block in the southeast. The SYG area is located near the western margin of the Yangtze Block and characterized by intersection of the NE-, NS- and NW-trending faults (Fig. 1). Distributions of the lead–zinc deposits are strongly restricted by the Emeishan basalts. Moreover, basalts and the lead–zinc deposits are controlled by faults that are not only the pathways for the ore-forming fluids, but also the locations where the ore minerals precipitated. The exposed stratigraphic sequences in this region comprise rocks from Archean (the Kunyang Group and Huili Group) to Quaternary, except the Cretaceous and Jurassic strata. Except the Quaternary, other layers, especially the Proterozoic, Cambrian, Devonian and Carboniferous sequences, host lead–zinc deposits completely (Han et al., 2007; Huang et al., 2010). A 100 km long and 40 km wide lead–zinc mineralization belt exists in the Proterozoic Dengying Group in the SYG, and the Jinshachang deposit is located in the north of this belt.

The Jinshachang lead–zinc district controlled by faults is located in the northwest of the SYG and at the intersection of the NE-trending Lianfeng fault and the secondary NW-trending Jinshachang reverse fault (F_1) (Fig. 2). In the west and north of this district, several gypsum mines are located on both sides of Yangtze River in the Lower Cambrian strata. The nearest Hekou gypsum mine is situated 4 km northwest of Jinshachang deposit and comprises some orebodies having thickness in the range of 1.6–11 m and length in the range of 190–1000 m. The ore minerals of the Hekou mine are shallow marine lacustrine sediments, consist of mainly gypsum and less amount of dolomite, and show blocky structure (Regional geological report, 1978).

Around this district, several hypogene hot springs are distributed in the Jinshajiang River valley. The water of springs is colorless, transparent and odorless or is slight odor and salty, and has high temperature ranging from 30° C to 50°C. The nearest spring is located 1km away from Jinshachang deposit and on the axis of the Jinshachang anticline (Fig. 2). Previous studies showed that the spring water collected from the Proterozoic dolomite had low contents of K^+, Na^+ and Cl^-, and relatively high contents of SO_4^{2-} and Ca^{2+}, indicating that the leaching soluble salts might be gypsum (Regional geological report, 1978). About 12 km northeast of this deposit, there is a primary hydrothermal copper mineralization spot related to the Emeishan basalts containing minerals of native copper, chalcopyrite and malachite. Other copper mineralization spots have also been detected not far from ore district.

2.2 Geological background of the deposit

The stratigraphic sequences at the Jinshachang district are the Early Proterozoic to Paleozoic strata, except the Devonian and Carboniferous strata (Fig. 2). The orebodies of this deposit occur mainly within the Meishucun Group

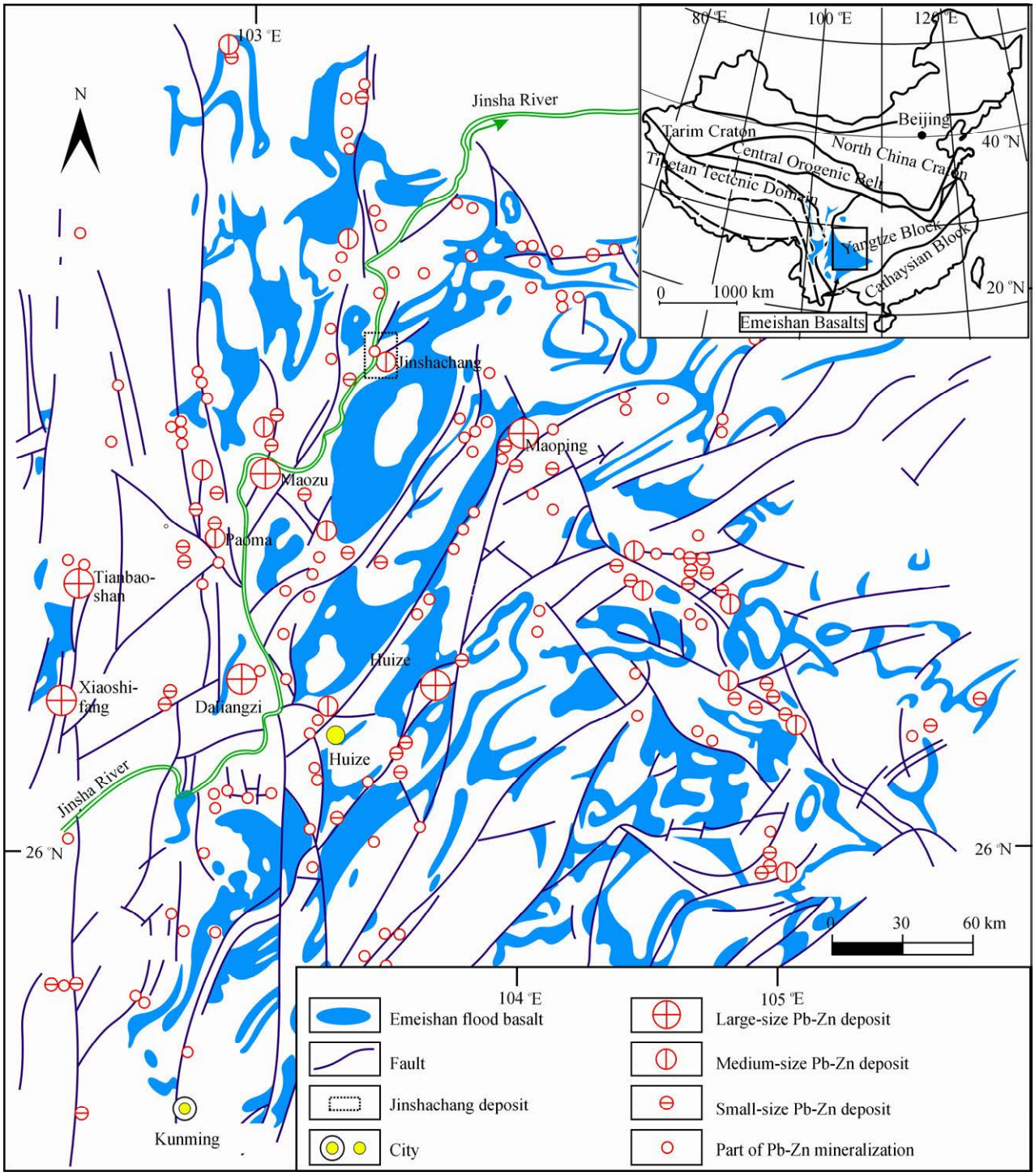

Fig. 1. Tectonic map of the Sichuan-Yunnan-Guizhou Pb-Zn polymetallic metallogenic province and distribution of the Pb-Zn deposits or mineralization pots (revised from Liu and Lin, 1999).

(the Lower Cambrian, including the Dahai, Zhongyicun and Xiaowaitoushan Formations, Shields et al., 1999) and the Upper Dengying Group (the Upper Neoproterozoic including the Baiyanshao and Jiucheng Formations, Shields et al., 1999) (Fig. 4). The Meishucun Group consists of a basal unit (~10 m thick) of light gray siliceous dolomite and an overlying unit (~27 m thick) of phosphorous dolomite. The 3.2 km long and 1 km wide Jinshachang deposit is hosted mainly in the Upper Dengying Formation (Baiyanshao Group), which is subdivided into the upper and lower dolomite units. The upper unit contains interbedded siliceous dolomite and gray–white microlite dolomite with typical laminated structures and wavy bedding. The lower rocks surround

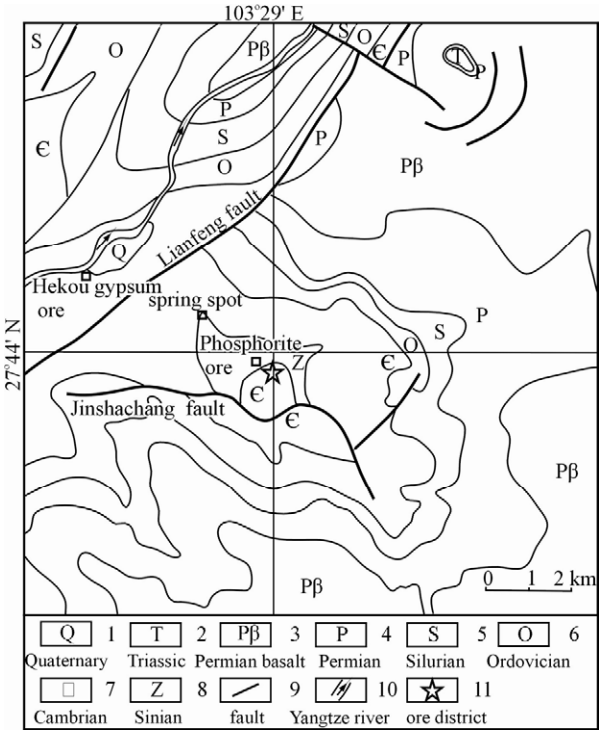

Fig. 2. Regional geological sketch map of Jinshachang Pb-Zn deposit and its surrounding district (after Pei, 1978)

lead–zinc orebodies and consist of light-gray cryptocrystal to fine-grained dolomite containing siliceous strips and corrosion holes mostly filled with limonite. The mine area has been divided into three oreblocks, from west to east: Yanshan oreblock, Guanfang oreblock and Jinshachang oreblock, respectively. No magma exists in the mine area, but it is surrounded by the Emeishan basalts. The geological structural feature of this deposit is characterized by a dome-like short-axis anticline and several faults (Fig. 3). Two main fault systems occur in this district. The Lianfeng deep fault trending northeast–southwest controlled the strata thickness and lithofacies paleogeography and underwent multiperiod activities. The Jinshachang fault, the secondary fault where ore minerals were precipitated, trends northwest–southeast, dips steeply to the northeast, and parallels the fold axis; it has an exposed length of 7 km and a width of less than 150 m.

3 Samples and Analytical Techniques

In this study, 65 sulfide samples, including separates of sphalerite, galena and pyrite, and eight sulfate samples, were analyzed for their sulfur isotopic compositions. All

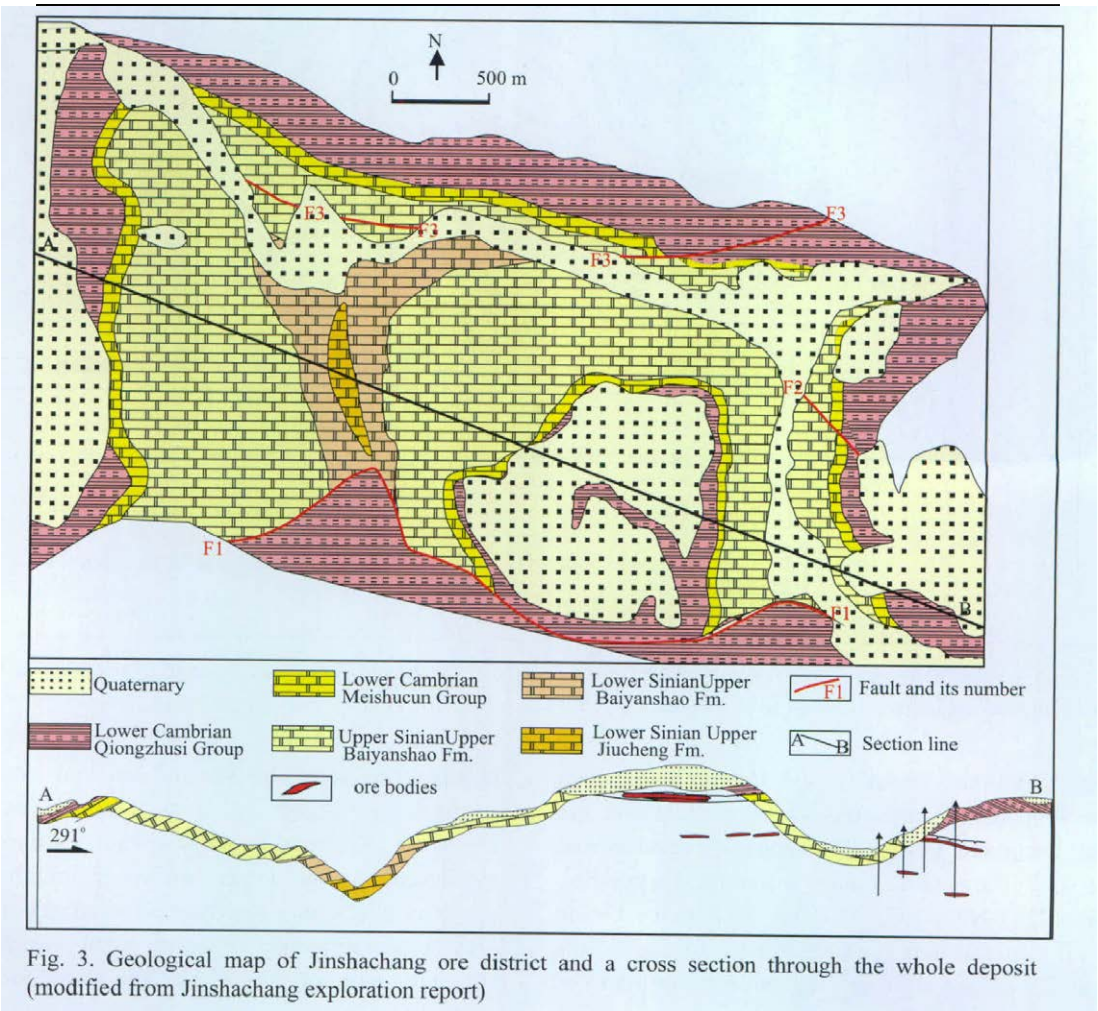

Fig. 3. Geological map of Jinshachang ore district and a cross section through the whole deposit (modified from Jinshachang exploration report)

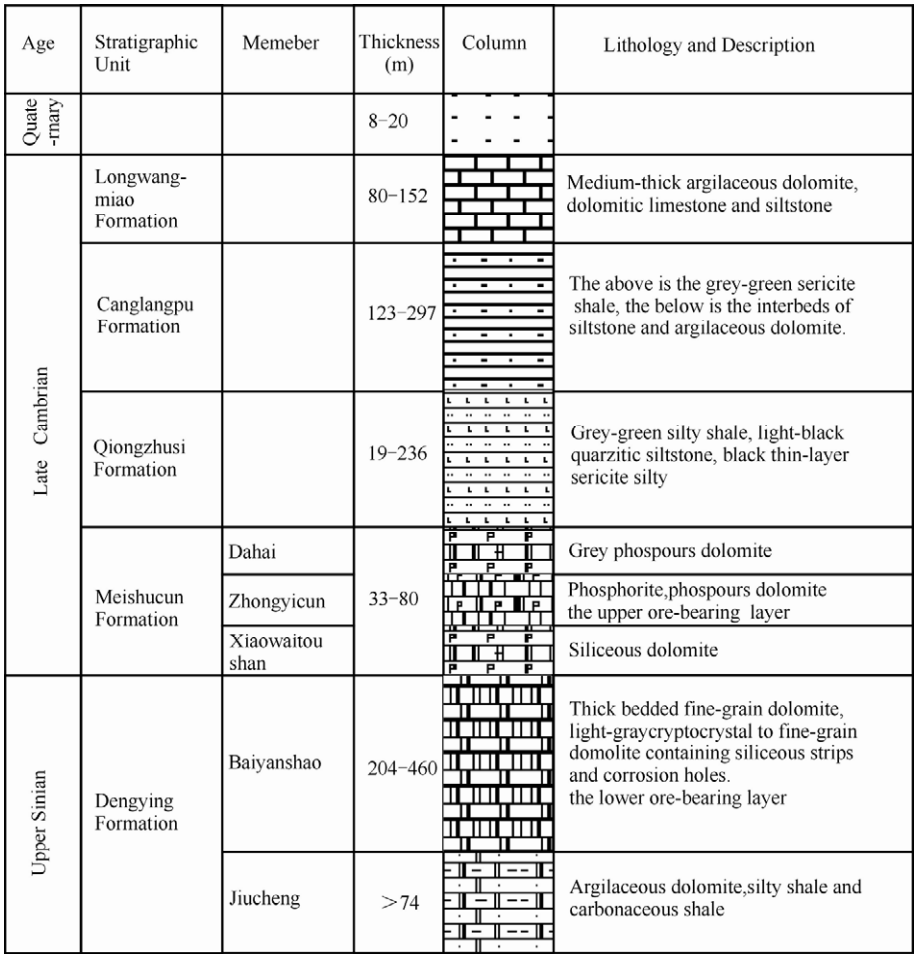

Fig. 4. Histogram of the strata of the Jinshachang Pb-Zn deposit

these samples were collected from main No. I_2, No.II, and No.IV orebodies of the Jinshachang deposit. Samples were handpicked under a binocular microscope to obtain 48 separates of sphalerite, 13 separates of galena, and 5 separates of pyrite. Sulfur isotopic compositions were analyzed using a Finnigan MAT-252 isotope ratio mass spectrometer at the Institute of Geochemistry, Chinese Academy of Sciences, and expressed in LTB-2 standard ($\delta^{34}S_{CDT}‰ = 1.84 \pm 0.2$) with a precision of ±0.2‰.

4 Results

4.1 Mineralogy and texture

Mineral components of the Jinshachang deposit were found to differ from other lead–zinc deposits in the SYG area but were similar to those of MVT type. This deposit was observed to comprise a major ore mineral assemblage of sphalerite and galena; a major gangue of barite, fluorite, quartz and dolomite; and less quantity of other minerals such as plumbojarosite, pyrophylite, bournonite, pyrite, kaolinite, argentite, chalcopyrite and calamine, hemimorphite, hydrozincite, cesusite, sardinianite, malachite, azurite and limonite. The ore minerals showed typical poikilitic and automorphic–hypidiomorphic granular textures, as well as massive, banded, disseminated, brecciated, vesicular and spotted structures. Minerals of sphalerite, galena and barite were often found to coexist and form an envelope (Fig. 5a, b, and 6d) in which barite and sphalerite surrounded each other, suggesting their coprecipitation (Fig. 6a, b, and c). The acid–sulfate type of alteration characteristics including solution holes (Fig. 5d) and vuggy silica cores were identified, which implies a magmatic environment. Some red crusty structural materials, including plumbojarosite, calcite, dolomite and pyrophylite, were found to locate in the matrix of quartz and dotted galena (Fig. 5c), which suggests that the former primary ore minerals partly suffered an oxidation process.

A paragenetic sequence was summarized on the basis of geological field studies and observations of hand specimens and thin sections. The stages defined primarily by the combined feature of sphalerite and galena and the alteration characteristics are summarized as follows: (1) early deposition of barite, sphalerite, quartz and fluorite;

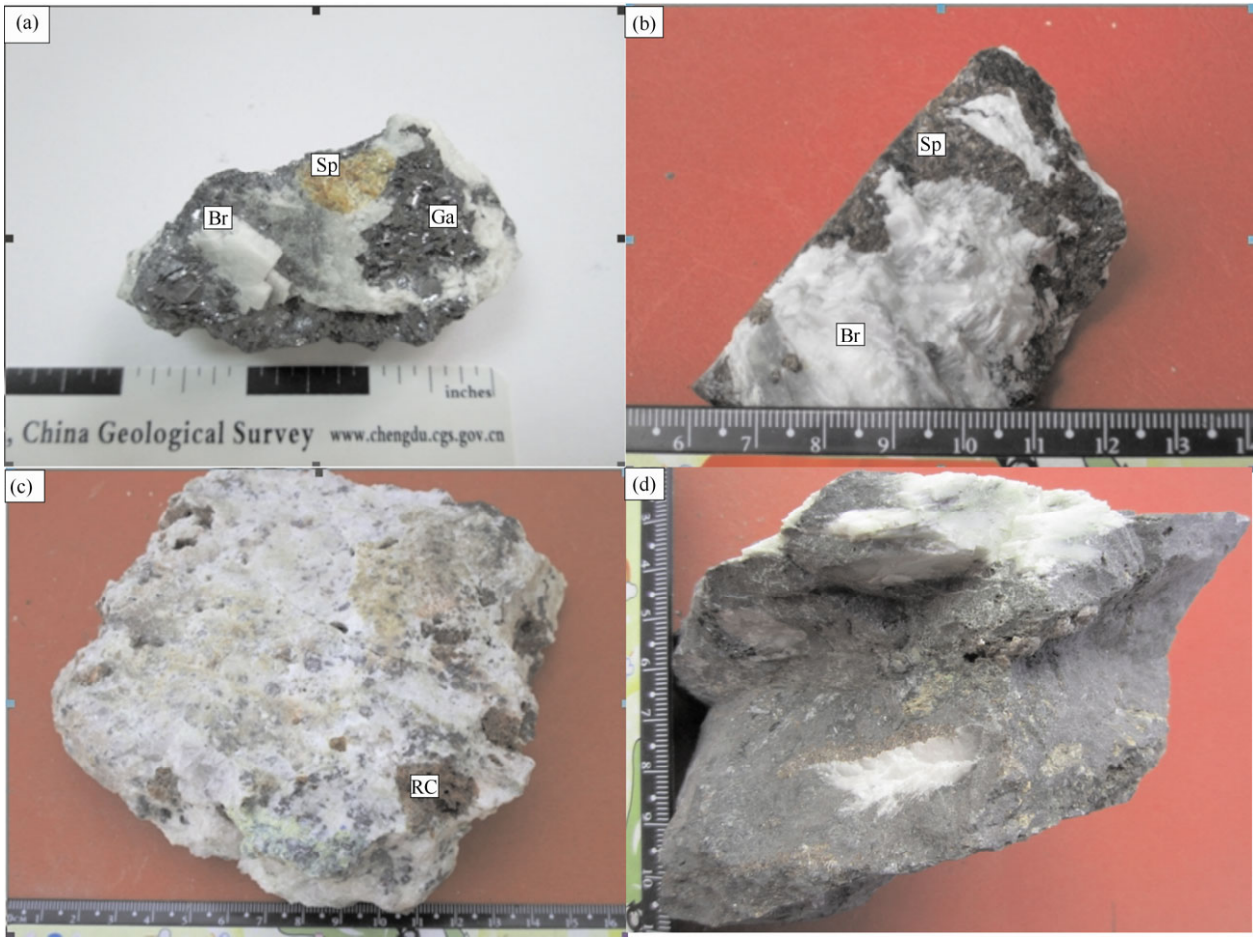

Fig. 5. Photographs showing the association relationship between minerals from Jinshachang Pb-Zn deposit.
(a) the barite and light sphalerite are included by galena (Sp, sphalerite; Ga, galena; Br, barite); (b) the sphalerite and barite coexist and are enveloped with each other; (c) red crusty structural material (RC) including plumbojarosite, calcite, dolomite and pyrophylite and (d) solution holes of the acid sulfate alterations.

(2) hydrothermal alteration of the formed mineral assemblages; and (3) formation of galena, fluorite, quartz and less amount of barite.

4.2 δ^{34}S values of sulfide and sulfate

In order to classify data more conveniently, sphalerite minerals were divided into three types according to their color: light, medium and dark. As shown in Table 1, the δ^{34}S values of sphalerite minerals fall in the coverage between 3.6‰ and 13.4‰ and have an average of 5.7‰. The δ^{34}S values of light-, medium-, and dark-colored sphalerite were estimated to be 4.7–13.4‰ with an average of 7.2‰, 4.5–12.3‰ with an average of 5.7‰, and 3.6–4.5‰ with an average of 4.1‰, respectively. Differences in δ^{34}S values between the lighter and the darker sphalerite minerals handpicked from samples 402-01, 401-7-3-04 and Jshch16 were relatively smaller than 0.4‰ which was twice the testing precision (±0.2‰), indicating that analytical errors might have resulted in the differences. However, differences in δ^{34}S values for samples 026-5-01, 401-7-3-03, 908Z-03 and 908-5-06 were 1.3‰, 4.3‰, 1.1‰ and 0.5‰, respectively, all of which were more than 0.4‰. Therefore, it can be concluded that sulfur isotopic values of the lighter sphalerite were more than those of the darker ones. Additionally, after excluding several larger δ^{34}S values of the light and medium types of sphalerite, the average δ^{34}S values were generally found to decrease from the lighter to the darker ones. Therefore, in the same specimen, the lighter color of sphalerite, the larger its δ^{34}S value. The δ^{34}S values of sphalerite present in orebodies were found to be notably distinct from those present in wall rocks. For example, δ^{34}S values of the light- and medium-type sphalerite present in wall rocks were 13.4‰ and 12.3‰, respectively. From the wall rocks to the inner zone of the orebodies, the δ^{34}S values decreased gradually from about 13.0‰ to 5.5‰. The δ^{34}S values of sphalerite that coprecipitated with galena in samples 105-202-06, 105-2-4-01 and Jshch23 were estimated to be 9.2‰, 9.3‰ and 11.2‰, respectively, with an average of 9.9‰.

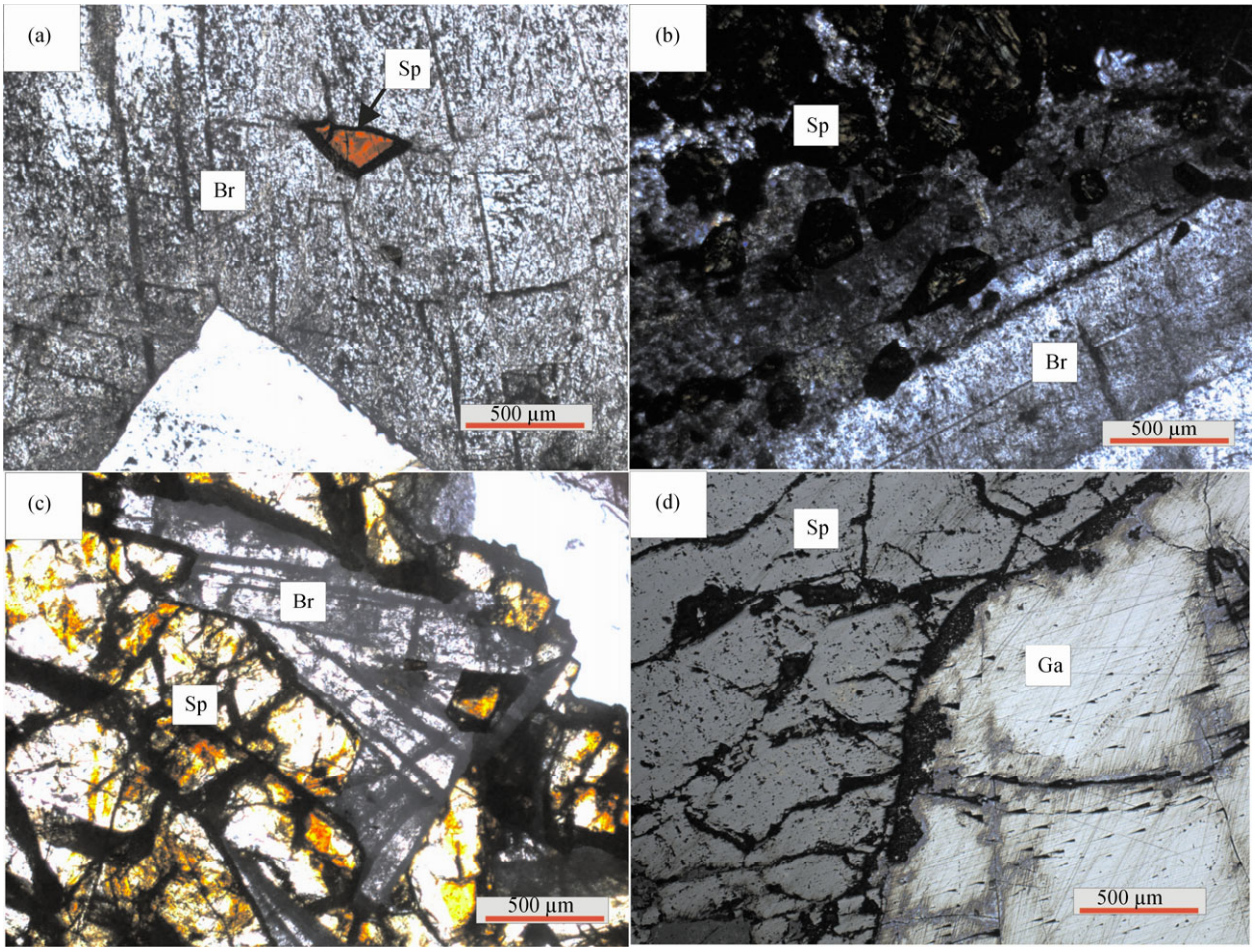

Fig.6. Microphotographs of ore minerals under single-polarized light (a, b, c) and reflected light (d).
(a) sphalerite (Sp) is embedded in the barite (Br); (b) granular sphalerites are included by barite; (c) long-strip barite is included by sphalerite and (d) co-precipitation of galena and sphalerite.

Apart from a δ^{34}S value of 3.7‰ in the sample Jshch24, the sulfur isotopic compositions of galena in other samples ranged from 6.0‰ to 9.0‰ (Table 1), with a total average value of 7.1‰. The average δ^{34}S value of galena from three fluorite–galena–sphalerite-type samples (6.5‰) was slightly smaller than the total average value, whereas that from altered dolomite containing covellite and aeruginosa (9.0‰) was larger than the total average value. The δ^{34}S values of pyrite were dispersed over an extraordinarily wide range, from −6.4‰ to 29.2‰ (Table 1), with typical isotopic characteristics of sedimentary pyrite. Pyrites hosted in the strata were observed to be patchy and pod-like aggregates, show finely granular structure, and have no symbiotic relationship with sphalerite and galena.

During this study, the coprecipitation phenomenon of barite, sphalerite and galena was very commonly observed, which is significant for discussing the source of sulfur. Therefore, it is necessary to analyze the sulfur isotopic compositions of barite. The δ^{34}S values of barite ranged from 32.1‰ to 34.7‰ (Table 1), with an average of 33.7‰. In the same specimen, the δ^{34}S values of sphalerite were found to be higher than that of galena, for instance, in samples 105-202-06, 105-2-4-01 and Jshch23, δ^{34}S values of the sphalerite were 9.2‰, 9.3‰ and 11.2‰, and those of the galena were 6.1‰, 6.1‰ and 8.2‰, respectively. This feature indicates that the sulfur isotopic compositions in the ore-forming fluids had partly reached isotopic equilibrium (Ohmoto, 1972).

4.3 Fluid inclusion data

In this deposit, two main types of inclusions in fluorite could be distinguished: (1) liquid–vapor inclusions (5.7–24 μm in size) and (2) vapor–liquid inclusions (7.2–32μm in size) (Fig. 7). Homogenization temperatures of inclusions were measured using a Linkam-THMSG600 at the Institute of Geochemistry, Chinese Academy of Sciences. The instrument can be used to measure temperatures over a range of 196–600°C with a precision of ±1° C. As shown in Table 2, homogenization temperatures of inclusions in fluorite were in the range 134–383°C and mostly consistent with the previous data.

Table 1 $\delta^{34}S$ values of sulfides and barite from the Jinshachang lead-zinc deposit

Sample	Mineral	Color	Color type	$\delta^{34}S$	Source	Sample	Mineral	Color	Color type	$\delta^{34}S$	Source
026-5-01-(1)	Sphalerite	light-yellow	light	6.0		908-4-02	Sphalerite	black	dark	3.6	
026-5-01-(2)	Sphalerite	red-brown	medium	4.8		908-5-03	Sphalerite	black	dark	4.1	
026-5-02-(1)	Sphalerite	light-yellow	light	4.7		908-5-05	Sphalerite	black	dark	4.1	
026-5-02-(2)	Sphalerite	red-brown	medium	4.8		908-5-06-(1)	Sphalerite	red-brown	medium	4.7	
026-5-03-(1)	Sphalerite	dark-brown	medium	4.7		908-5-06-(2)	Sphalerite	black	dark	4.2	
026-5-03-(2)	Sphalerite	red-brown	medium	4.9		105-202-01	Galena			6.0	
402-01-(1)	Sphalerite	light-yellow	light	5.0		105-202-04	Galena			7.5	
402-01-(2)	Sphalerite	red-brown	medium	4.8		105-202-06	Galena			6.1	
402-01-(3)	Sphalerite	black	dark	4.6		105-2-4-01	Galena			6.1	
402-03-(1)	Sphalerite	red-brown	medium	4.7		105-2-4-02	Galena			6.3	
402-03-(2)	Sphalerite	black	dark	4.3		889-02	Galena			7.1	This paper
401-7-3-02	Sphalerite	black	dark	4.1		889-05	Galena			9.0	
401-7-3-03-(1)	Sphalerite	light-yellow	light	8.5		889-06	Galena			8.6	
401-7-3-03-(2)	Sphalerite	black	dark	4.2		889-07	Galena			7.7	
401-7-3-04-(1)	Sphalerite	red-brown	medium	4.6		889-08	Galena			7.4	
401-7-3-04-(2)	Sphalerite	black	dark	4.4		Jshch23	Galena			8.2	
401-7-3-06	Sphalerite	black	dark	4.5		Jshch24	Galena			3.7	
105-202-06	Sphalerite	red-brown	medium	9.2		Jshch26	Galena			8.2	
105-202-07	Sphalerite	light-yellow	light	9.2		908-2-05	Pyrite			8.9	
105-2-4-01	Sphalerite	brown,yellow	light,medium	9.3		908-4-02	Pyrite			-6.4	
Jshch15	Sphalerite	light-yellow	light	5.0	This paper	Jshch16-1	Pyrite			26.0	
Jshch16-(1)	Sphalerite	red-brown	medium	4.8		Jshch16-2	Pyrite			1.7	
Jshch16-(2)	Sphalerite	red-brown		4.4		Jshch18	Pyrite			29.2	
Jshch20	Sphalerite	red-brown	medium	4.8		YJ3-1	Sphalerite			7.0	
Jshch23	Sphalerite	brown,yellow	light,medium	11.2		YJ3-2	Sphalerite			6.5	Tu (1984)
Jshch25	Sphalerite	light-yellow	light	6.7		YJ4-1	Galena			3.8	
908Z-02-(1)	Sphalerite	light-yellow	light	5.6		YJ4-2	Sphalerite			6.5	
908Z-02-(2)	Sphalerite	red-brown	medium	5.0		YJ6-1	Galena			7.0	
908Z-02-(3)	Sphalerite	black	dark	4.3		PbS-J-201	Galena			1.1	
908Z-03-(1)	Sphalerite	yellow	light	5.2		PbS-G-202	Galena			4.8	
908Z-03-(2)	Sphalerite	red-brown	medium	4.8		Pb-Y-211	Galena			2.6	
908Z-03-(3)	Sphalerite	black	dark	4.0		S-1-405	Sphalerite			4.6	Liu and Lin (1999)
908-1-01-(1)	Sphalerite	light-yellow	light	13.4		S-2-405	Galena			5.1	
908-1-01-(2)	Sphalerite	red-brown	medium	12.3		S-3-201	Sphalerite			4.7	
908-1-02-(1)	Sphalerite	light-yellow	light	8.6		S-4-201	Galena			2.3	
908-1-02-(2)	Sphalerite	red-brown	medium	9.1		S-5-105	Sphalerite			6.1	
908-1-03-(1)	Sphalerite	light-yellow	light	5.3		S-6-201	Sphalerite			4.7	
908-1-03-(2)	Sphalerite	red-brown	medium	5.8		401-7-3-06	Barite			34.7	
908-2-01	Sphalerite	red-brown	medium	4.5		908 中-03	Barite			33.3	
908-2-03	Sphalerite	red-brown	medium	4.7		908-2-01	Barite			32.1	This paper
908-2-05	Sphalerite	red-brown	medium	5.7		908-2-03	Barite			35.2	
908-3-02	Sphalerite	black	dark	4.1		908-3-02	Barite			32.9	
908-4-01	Sphalerite	black	dark	4.0		908-5-03	Barite			34.0	

5 Discussion

Distribution of $\delta^{34}S$ values could provide useful information on the material source, precipitation mechanisms of sulfide, and isotopic equilibrium among sulfur-bearing minerals (Arnold and Sheppard, 1981; Cazanas et al., 2003; Rye and Ohmoto, 1974). Coprecipitation phenomena of sulfur-bearing minerals and the narrow $\delta^{34}S$ values range of sulfides and barite make this deposit different from most of the lead–zinc deposits in the SYG area.

5.1 Source of sulfur in barite

In this study, the analyzed $\delta^{34}S$ values of barite ranged from 32.1‰ to 34.7‰, with an average of 33.7‰, and were consistent with the published isotopic data ($\delta^{34}S \approx$ 34.4‰) of sulfate from the Lower Cambrian and the Upper Sinian strata (Liu and Lin, 1999). Absence of the $\delta^{34}S$ values of sulfate from the Cambrian strata in this district restricted the discussion of data. However, Shields (1999) had reported the sulfur isotopic compositions of phosphate-bound sulfates from the Meishucun section (Lower Cambrian) in Yunnan province and several correlative sections in South China. Sulfates from the Meishucun section yielded tightly concentrated $\delta^{34}S$ values with an average of 33‰ (Shields et al., 1999), which coincide with the published $\delta^{34}S$ values (between 30 and 35 per mil) of evaporite from the Lower Cambrian

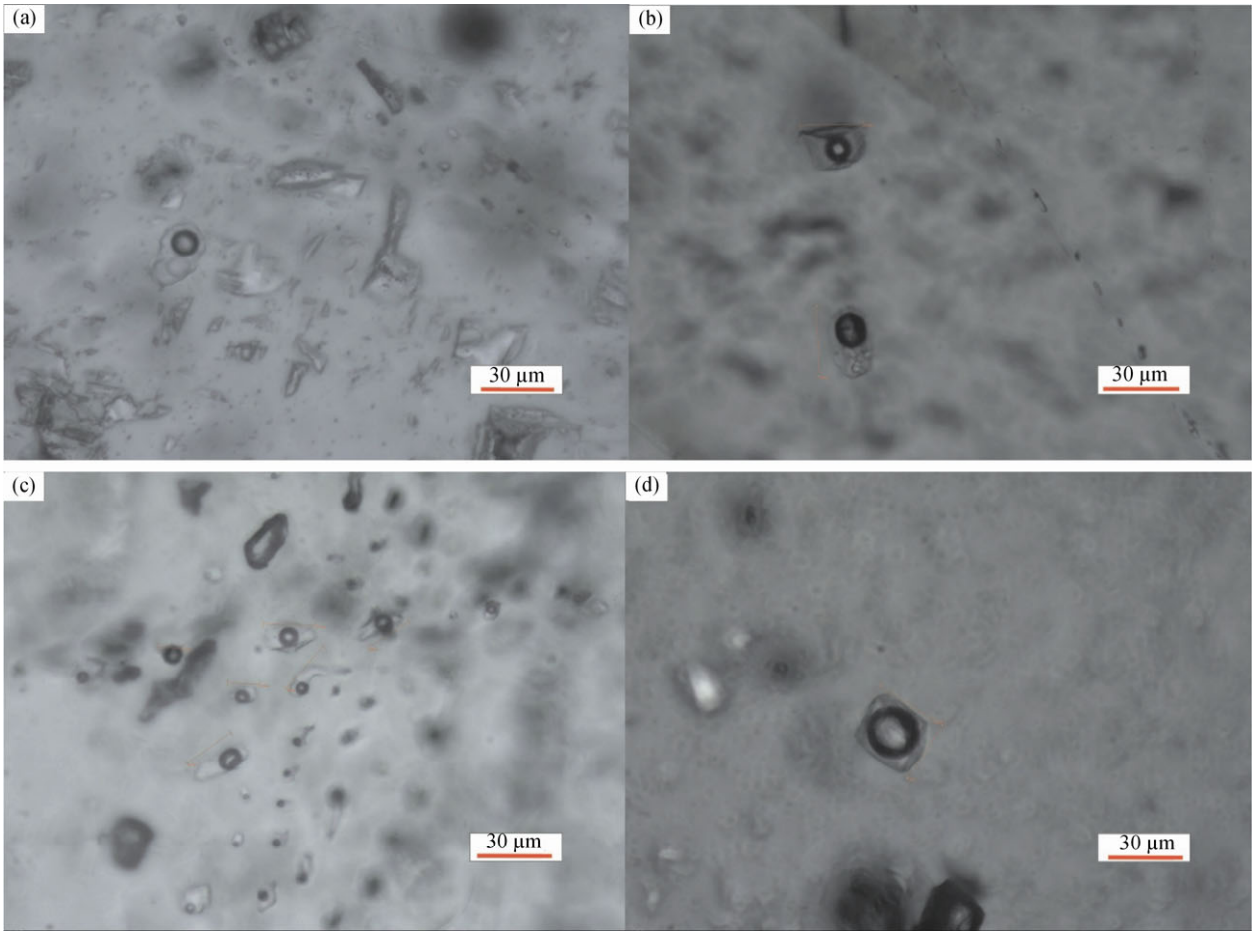

Fig. 7. Fluid inclusions in fluorite from the Jinshachang Pb-Zn deposit.
(a) liquid-vapour inclusion under temperature of -12℃: (b, c) liquid-vapour inclusions. (d) vapour-liquid inclusion

and the Upper Proterozoic strata in Siberia and elsewhere (Claypool et al., 1980), but almost all $\delta^{34}S$ values of sulfates from other strata were below 30‰ and less than the values of sulfates from near Neoproterozoic–Cambrian sections (Claypool et al., 1980; Shields et al., 1999). Therefore, the $\delta^{34}S$ values of barite are consistent well with that of sulfates from strata. Then considering that previous studies reported only about +1.65‰ fractionation between evaporite and barite (Liu and Bao, 2009; Thode and Monster, 1967), it suggested that the sulfur of barite came from the Lower Cambrian strata.

Significant amount of Emeishan basalts were found near the ore district, making it necessary to prove whether the sulfur of barite was derived from magnetic activities. Moreover, the presence of acid-sulfate type of alterations including solution holes, vuggy silica cores, kaolinite, covellite and pyrite in this deposit might indicate that it was the formed in a magmatic hydrothermal environment (Rye et al., 1992). However, the characteristic mineral of alunite had not been determined, mostly because it had been exhausted during sulfate reduction process or existed at greater depths. The red mineral assemblages containing plumbojarosite and pyrophylite in alteration holes may indicate the existence of alunite. In a magmatic hydrothermal environment, condensation of a magmatic vapor plume at intermediate depths may result in disproportionation of magmatic SO_2 reacting with H_2O to produce H_2S and H_2SO_4 (Holland, 1965; Rye et al., 1992). This mechanism often causes sulfur isotopic fractionation between sulfide and sulfate in the range of 16‰–28‰, and generates H_2SO_4 having $\delta^{34}S$ values generally below 28‰ and high H_2S/H_2SO_4 ratios (Rye, 1993; Rye et al., 1992). However, the average $\delta^{34}S$ value of barite was found to be about 34‰, confirming that the sulfur of barite could not have originated from a magmatic hydrothermal system. Atmospheric oxidation of H_2S released by boiling of deeper fluids could produce H_2SO_4 with the similar $\delta^{34}S$ values as that of the parental H_2S (Field and Lombardi, 1972; Lombardi and Sheppard, 1977); however, in this deposit differences in $\delta^{34}S$ values between sulfides and barite were up to 31‰, indicating that this mechanism could not generate such amount of sulfur of barite. Therefore, it was suggested that the sulfur of barite was derived from the Lower Cambrian and Upper

Proterozoic strata. Additionally, several salt springs with high concentrations of SO_4^{2-} and Ca^{2+} ions were found near this deposit, which might be a result of leaching and active migration of gypsum in this region.

Surprisingly, in the SYG area, most of the lead–zinc deposits containing less or no barite, such as the Huize, Maping and Maozu deposits, are mostly hosted in the Upper Paleozoic strata; however, some deposits containing voluminous barite, such as the Jinshachang, Lehong and Wuxingchang deposits, are mostly hosted in the Cambrian and the Upper Sinian strata. Based on above fact and discussions, it suggest that the sulfur of barite was mainly derived from the Cambrian and the Upper Sinian strata in lead–zinc deposits having significant amount of this mineral and less originated from the Upper Paleozoic strata in the SYG area. Also, depletion of sulfate in upward fluids due to its thermochemical reduction was thought to account for the less barite in the deposits hosted in the Upper Paleozoic strata.

5. 2 Source of sulfur in sulfide

The $\delta^{34}S$ values of about 80% of sphalerite were estimated to be between 3.6‰ and 6.0‰ (Fig. 8) and the $\delta^{34}S_{\Sigma S}$ values of ore-forming fluids were between 3.0‰ and 6.5‰ (Liu and Lin, 1999), which are close to that of sulfur from a deeply seated source (Tu, 1984). However, sulfur of sulfides (Fig. 8) in the Huize (Li et al., 2006) and Maozu (Guo, 2011; Liu and Lin, 1999) deposits were shown to have been derived from the strata due to thermochemical reduction of sulfate. On the basis of the findings that sphalerite predominantly coexisted with barite in orefields, several gypsum ore pots were hosted in the Lower Cambrian strata, and gypsodolomite were discovered in the drilling holes, it suggested that the sulfur of sphalerite and galena originated from the strata through thermochemical reduction of sulfate.

Two effective mechanisms of sulfate reduction, including bacterial sulfate reduction (BSR) and thermochemical sulfate reduction (TSR), have so far been reported (Machel, 1989; Seal, 2006). The BSR process typically occurs at the temperature lower than ~110°C (Basuki et al., 2008; Jørgensen et al., 1992; Mitchell et al., 2009); the reducible sulfur produced by this mechanism is characterized by a dispersed distribution of $\delta^{34}S$ values (Dixon and Davidson, 1996; Sim et al., 2011). The $\delta^{34}S$ values of sulfides generally fall in a narrow range and the homogenization temperatures of fluid inclusions in fluorite and barite ranged from 134°C to 383°C and from 178°C to 293°C, respectively (Table 2), which exceed the temperature suitable for the BSR. Therefore, BSR mechanism could not be an efficient path for the production of reduced sulfur in this district. The TSR

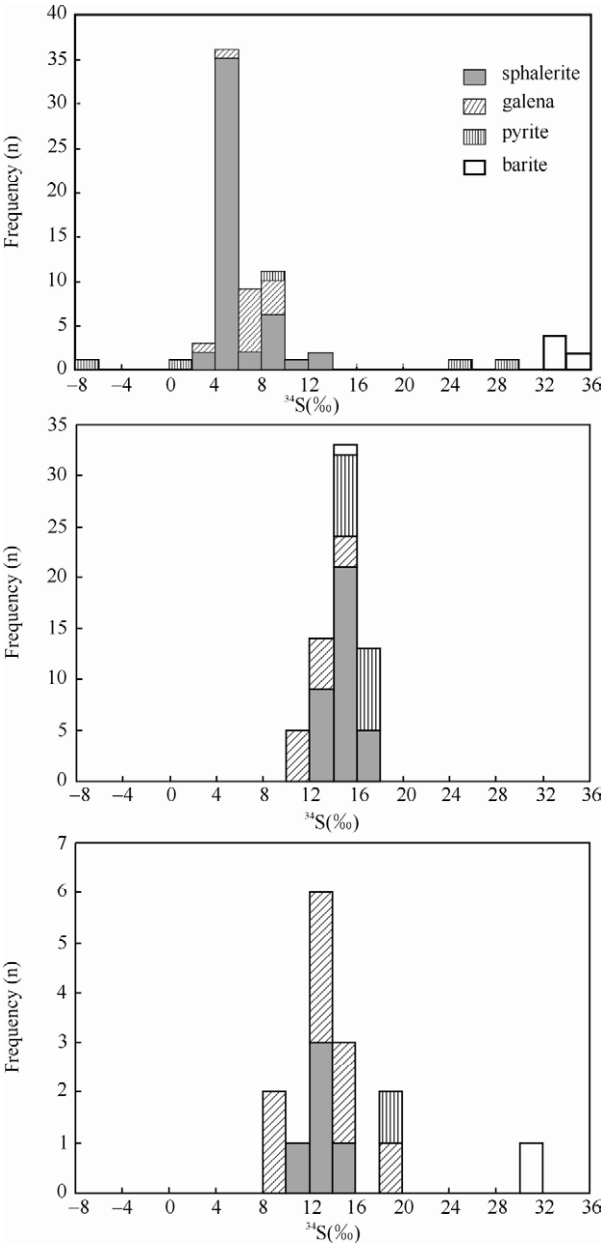

Fig. 8. Histogram of $\delta^{34}S$ values of sulfur-bearing minerals from the Jinshachang (a), Huize (b) and Maozu(c) Pb-Zn deposit.

mechanism occurs at temperatures in excess of 100–135°C (Machel, 1989) and becomes more rapid and effective above a temperature of 175°C (Dixon and Davidson, 1996). This process can generate large amount of reduced sulfur with a concentrated distribution of $\delta^{34}S$ values and may cause isotopic fractionations in the range from ~0 to ~20 per mil between sulfides and sulfates (Kiyosu and Krouse, 1990; Machel et al., 1995). If the reduced sulfur in this deposit was derived from sulfates of the Lower Cambrian or Upper Neoproterozoic strata, sulfur isotopic fractionation during sulfate reduction would have been less than 20‰ and the sulfur of sphalerite and galena

Table 2 Homogenization temperature of inclusions in fluorite, barite and quartz

Inclusion sample	Mineral	Number	Homogenization temperature(℃)	Average temperature(℃)	Source
Jshch23	fluorite	23	134~383	173	This paper
401-7-3-01	fluorite	6	141~190	178	
401-7-3-03	fluorite	10	162~303	204	
908-2-02	fluorite	10	211~317	275	
908-2-04	fluorite	12	145~351	209	
Jin4-1	fluorite		107~195	139	(Liu and Lin,1999)
BTY-211-B	fluorite	3	84~130	114	(Liu,1989)
BTG-202	fluorite	13	152~227	211	
BTY-211-E	fluorite	14	173~301	245	
BTG-207	fluorite	17	134~350	291	
BTJ-201-A	fluorite	17	153~293	209	
BTJ-402-B	fluorite	14	91~266	172	
BTG-202	barite	11	178~293	235	
BTJ-201	quartz	16	126~261	184	

should have had a minimum δ^{34}S value of 13‰. The δ^{34}S values of sulfides in the Jinshachang deposit were reported to be mostly below 13‰, therefore, the sulfur of sulfides in this deposit did not originate completely from strata. Sulfate is also present in the Lower Silurian strata in this district, but at present no sulfur isotope data for evaporitic sulfates from the SYG area is available. Claypool (1980) reported only one δ^{34}S value (28.2‰) of sulfate from the Lower Silurian strata; therefore, if the TSR process would have occurred, the sulfur of sphalerite and galena should have preserved a minimum δ^{34}S value of 8‰. Consequently, the sulfur of sulfides was not derived mainly from the Silurian strata.

On the basis of similar δ^{34}S values of sulfides (δ^{34}S≈+10 to +16‰) in the Huize lead–zinc deposit and sulfates (δ^{34}S≈+16‰) in the Carboniferous strata, Han (2006) and Li (2006) suggested that the sulfur of sulfides was a result of contribution by marine sulfates and possible incorporation of sulfur from deep-seated sources. Recently, they proposed that the sulfur of sulfides was derived from sulfates of a gypsum bed present in the hosted stratum, which might be a plausible explanation because the δ^{34}S values of reduced sulfur generated by thermochemical reduction of sulfate in the Lower Cambrian or Upper Neoproterozoic strata should be similar to those of sulfides from the Huize deposit. On the other hand, δ^{34}S values of the reduced sulfur generated from sulfates of the Carboniferous and Devonian strata through TSR mechanism should be similar to those of sulfides from this deposit. However, in this study, it is difficult to confirm that the sulfur of sulfide was derived from the Carboniferous and Devonian strata, because of the following factors: 1) Han (2012) attributed the formation of lead–zinc deposits in the northeast of the Yunnan province to the transformation mechanism between the extensional environment in the Late Hercynian and the orogenic compression environment in the Indosinian period; 2) Zhang (1997) had proved that the mineralization of the lead–zinc deposit in the SYG area possibly occurred in the Late Permian, the same period as the occurrence of the Emeishan basaltic eruption event; 3) no Carboniferous and Devonian strata were found in or near the ore district.

Drummond (1981) and Ohmoto and Lasaga (1982) suggested that the coprecipitation of sulfides and sulfates should result from the mixing of sulfides- and sulfates-rich solutions, especially when a temperature difference exists between these two solutions. They stressed that this mechanism is very effective for the coprecipitation of both sulfate and sulfide minerals. Considering the prevalent coexistence of sulfate and sulfides, sulfur isotopic features of sulfides, and consistent sulfur isotopic values between barite and evaporite in this deposit, it is believed that mixing of the two solutions was an important mechanism for the formation of orebodies and that the relatively cold solution was the sulfates-rich solution leaching from strata while the relatively hot solution was the sulfides-rich solution related to the magmatic activities.

The sulfur isotopic compositions of hydrothermal sulfides of many deposits related to magmatic activities was rather low. Richardson (1988) showed that the hydrothermal sphalerite of Deardorff mine had δ^{34}S values of 4.0–8.9‰ and attributed sulfur source to petroleum and possible igneous or crustal sulfur from the basement. Sulfides from the Ladolam hydrothermal gold deposit were found to preserve sulfur isotope values of −12.9‰ to +3.6‰, consequently, it was considered that the magmatic volatiles had significant amount of sulfur to systems (Gemmell et al., 2004). In the ELIP, the δ^{34}S values of sulfides from Ni–Cu–PGE (Platinum Group Elements) deposits related to Emeishan basalts were between 2.4 and 5.4 per mil, which was little above that of mantle sulfur. It suggested that two processes accounted for the increase in δ^{34}S values of mantle sulfur: the crustal material contamination and the interfusion of marine sulfates (Ma, 2009). All these values were almost consistent with that of

sphalerite from this deposit and near the values of mantle sulfur. Therefore, this study speculate that the reduced sulfur of the Jinshachang deposit were mainly derived from mantle, which is also consistent with the study of Tu (1984). More importantly, the δ^{34}S values of sulfides from the Tianbaoshan Pb–Zn deposit mostly ranged from 0‰ to 5‰ and coincided with those of the Jinshachang deposit. The Tianbaoshan deposit had the Pb+Zn reserves of above 1 Mt (Wang et al., 2000) and was also hosted in the Dengying Group in the SYG area. The sulfur isotopic compositions of sulfides in the Tianbaoshan deposit agreed well with that of the deposit formed in a magmatic hydrothermal environment, thus Gao and Luo (1999) considered that intrusions of igneous rock played an advanced role in the formation of the deposit. Similarly, the low δ^{34}S values of sulfides for the Jinshachang deposit should be related to Emeishan magmatic activity that drove the ore-forming fluids upward, as Zhang (1997) had proposed.

Factually, huge quantities of sulfur had released from mantle to the ocean atmosphere due to an asteroid or a comet hitting the ocean in the Late Permian (Kaiho et al., 2001). This catastrophic event occurred about several million years after the main eruption phase of Emeishan basalts, i.e., 259 ± 3 Ma (Zhou et al., 2002). During the eruption of basalts, mantle fluids including CO_2, H_2O, H_2S, SO_2 and other compositions emitted, which provided materials and heat for deposits (Liu et al., 2001). Integrating some information that the features of sulfur isotopic composition, ore district being surrounded by basalts, mineralization possibly occurring in the Late Permian (Zhang, 1997), and lead–zinc deposits mostly hosting below or very few inside the Emeishan basalts, it suggested that the reduced sulfur of the Jinshachang deposit was derived mainly from mantle and mixed with the sulfur of sulfates from strata during the eruption of Emeishan basalts.

5.3 Sulfur isotopic equilibrium temperature

Generally, the δ^{34}S values of sphalerite are lower than that of galena, which implies that the sulfur had not reached isotopic equilibrium, mostly because of the coexistence of different minerals and the existence of multiphase ore-forming fluids in the deposit. However, in the same specimens, the δ^{34}S values of sphalerite were always found to be higher than those of galena, indicating that the sulfur had attained isotopic equilibrium in ore-forming fluids. Therefore, the galena–sphalerite and sphalerite–barite pairs were used to calculate the sulfur isotopic equilibrium temperature employing the formula presented by Seal (2006). The equations are shown as follows and the factors are given in Table 3.

$$1000\ \mathrm{In}\alpha_{\text{i-}H_2S} = \frac{a\times10^6}{T^2} + \frac{b\times10^3}{T} + \mathrm{c}; \quad (T \text{ in K}) \tag{1}$$

$$1000\ \mathrm{In}\alpha_{\text{i-}H_2S} \approx \Delta_{\text{i-}H_2S} \tag{2}$$

As shown in Table 4, the sulfur isotopic equilibrium temperatures of sphalerite–galena pairs ranged from 204° C to 220°C and fell in the range of homogenization temperatures (178–293°C) of fluid inclusions, as shown in Table 2. Ohmoto and Lasaga (1982) explained that the chemical equilibrium between aqueous sulfates and sulfides was difficult to attain during the coprecipitation process at the temperature below 350°C, but if the cooling rate of fluids were rather low, this could be attained even at the temperature as low as 200°C. Factually, heating of the overlying crust by the underplated or intruded basaltic magma during magmatic activities can slow the cooling rate of hydrothermal fluids (Annen et al., 2006; Annen and Sparks, 2002; Huppert and Sparks, 1988). Therefore, sulfur isotopic equilibrium temperatures of sphalerite–barite pairs were calculated. The results showed that temperatures were in the range 190–212° C, which matched with the range of the homogenization temperature of fluid inclusions, indicating that the sulfur isotope between sphalerite and barite should have attained equilibrium.

5.4 Migration model of reduced sulfur

In this study, the darker sphalerite minerals were found to have more FeS content (Liu and Lin, 1999) and lower δ^{34}S value, which coincided with that shown by Peevler (2003) regarding sphalerite, but were opposite to that the darker sphalerite having higher δ^{34}S value in the SYG area shown by Li (2006) and Zhou (2010). According to the mineralogical data that the darker sphalerite had precipitated earlier than the lighter ones and the sulfur

Table 3 Equilibrium isotopic fractionation factors for sulfide minerals and related compounds described by the equation l

Component (i)	a	b	c	temperature range (°C)	Source
Sulfate	6.46	0	0.6	200~400	(Ohmoto and Lasaga, 1982)
PbS	-0.6	0	0	50~700	(Ohmoto and Rye, 1979)
ZnS	0.1	0	0	50~705	(Ohmoto and Rye, 1979)

Table 4 Equilibrium temperature between sulfur-bearing minerals calculated by the equation

Sample	Sphalerite δ^{34}S (‰)	Galena δ^{34}S (‰)	Barite δ^{34}S (‰)	Equilibrium temperature (°C)
Jshch23	11.2	8.2		220
105-202-06	9.2	6.1		212
105-2-4-01	9.3	6.1		204
401-7-3-06	4.5		34.7	190
908Z-03	4.7		33.3	203
908-2-01	4.5		32.1	212
908-2-03	4.7		35.2	188
908-3-02	4.1		32.9	202
908-5-03	4.1		34.0	193

isotopic features, the $\delta^{34}S$ values of S^{2-} ions in ore-forming fluids should become higher with the reduced sulfur produced by the TSR process continually entering into the ore-forming fluids. The $\delta^{34}S$ values of sphalerite near wall rocks were found to be up to 13‰ and decreased dramatically while approaching the inner zone of orebodies. This can be interpreted as that S^{2-} ions diffused in the limited region during the mixing of two different solutions, because the TSR process of sulfates took place in wall rocks at the same time when the ore-forming fluids heated the surrounding rocks. The sulfur isotopic fractionations between sulfides and sulfates could be up to 20‰ under a temperature of 100°C, therefore, the input of sulfur from sulfates into fluids could account for the higher $\delta^{34}S$ values of sphalerite close to the orebodies. Two higher $\delta^{34}S$ values of sphalerite in dolomite presented by Liu and Lin (1999) ($\delta^{34}S \approx 19.5‰$ and 24.6‰) should also be related to the TSR process.

Galena precipitated in lower elevation than sphalerite had higher $\delta^{34}S$ value, because as the ore-forming fluids evolved the $\delta^{34}S$ of reduced sulfur increased. Therefore, a simple model was proposed, which would include two stages of the evolution of reduced sulfur in ore-forming fluids. In the first stage, the upward hot sulfides-bearing solution (or H_2S-bearing solution) mixed with the cold sulfates-bearing solution (or SO_4^{2-}-bearing solution), followed by the precipitation of certain amounts of sphalerite and galena. In this stage, the sulfates from strata or magmatic systems began to be reduced. In the second stage, SO_4^{2-} irons were reduced to S^{2-} through the TSR process and entered the fluids, and then S^{2-} combined with Pb^{2+} from strata to form galena. The appearance of late lighter sphalerite and barite included in galena validated this interpretation (Fig. 5a).

6 Conclusions

In Jinshachang lead-zinc deposit, the sulfur of barite mainly originated from the marine sulfates of the Lower Cambrian and Upper Proterozoic strata. The reduced sulfur of sulfides was mainly related to magmatic activities and suffered contamination by crustal sulfur and reduced sulfur produced by TSR. The coprecipitation of sulfides and sulfates can be interpreted as a result of mixing of the hot sulfides-bearing solution and the cold sulfates-bearing solution. The cold sulfates-bearing solution originated from strata. However, hot sulfides-bearing solution was related to magmatic activities, which was supported by the high homogenization temperature of inclusions and the little differences in $\delta^{34}S$ values between sphalerite in this study and other sulfides associated with magma in the SYG area. In the beginning, mixing of the two solutions resulted in the coprecipitation of barite with $\delta^{34}S$ values similar to those of sulfates from strata, and sphalerite with low $\delta^{34}S$ values. Next, the $\delta^{34}S$ values of reduced sulfur in ore-forming fluids increased owing to the TSR process, resulting in high $\delta^{34}S$ values of sphalerite and galena that were produced later.

This model can explain the feature of sulfur isotopic compositions of sulfur-bearing minerals and special mineral association in the Jinshachang lead–zinc deposit. Moreover, it may shed new light on the future investigations related to the possibility of mineralization in deep and fault-developed areas.

Acknowledgements

This work is granted by the Key Research Program of the Chinese Academy of Sciences (KZCX2-YW-Q04-05) and a Special Research Fund of the SKLOG, IGCAS (KCZX20090103). We thank Ning An in Institute of Geochemistry, Chinese Academy of Sciences for measuring sulfur isotopic composition and the geologists in the Jinshachang lead-zinc deposit for their help during the field investigation.

Manuscript received Nov. 1, 2012
accepted Mar. 21, 2013
edited by Fei Hongcai

References

Annen, C., Scaillet, B., and Sparks, R.S.J., 2006. Thermal constraints on the emplacement rate of a large intrusive complex: The manaslu leucogranite, nepal himalaya. *Journal of Petrology*, 47: 71–95.

Annen, C., and Sparks, R.S.J., 2002. Effects of repetitive emplacement of basaltic intrusions on thermal evolution and melt generation in the crust. *Earth and Planetary Science Letters*, 203: 937–955.

Arnold, M., and Sheppard, S.M.F., 1981. East Pacific Rise at latitude 21° N: isotopic composition and origin of the hydrothermal sulphur. *Earth and Planetary Science Letters*, 56: 148–156.

Basuki, N.I., Taylor, B.E., and Spooner, E.T.C., 2008. Sulfur isotope evidence for thermochemical reduction of dissolved sulfate in Mississippi Valley-tye zinc-lead mineralization, Bongara area, northern Peru. *Economic Geology*, 103: 783–799.

Cazanas, X., Alfonso, P., Melgarejo, J.C., Proenza, J.A., and Fallick, A.E., 2003. Source of ore-forming fluids in El Cobre VHMS deposit (Cuba): evidence from fluid inclusions and sulfur isotopes. *Journal of Geochemical Exploration*, 78–9: 85–90.

Claypool, G.E., Holser, W.T., Kaplan, I.R., Sakai, H., and Zak, I., 1980. The age curves of sulfur and oxygen isotopes in marine sulfate and their mutual interpretation. *Chemical Geology*, 28: 199–260.

Dixon, G., and Davidson, G.J., 1996. Stable isotope evidence for

thermochemical sulfate reduction in the Dugald river (Australia) strata-bound shale-hosted zinc-lead deposit. *Chemical Geolog*, 129: 227–246.

Drummond, S.E., 1981. *Boiling and mixing of hydrothermal fluids: Chemical effects on mineral precipitation.* The Pennsylvania State University (Ph.D thesis).

Field, C., and Lombardi, G., 1972. Sulfur isotopic evidence for the supergene origin of alunite deposits, Tolfa district, Italy. *Miner. Depos*, 7: 113–125.

Gao Jianguo and Luo Jiangping, 1999. Contrasting analysis on the ore forming process of east and west orebody of HuiLi Pb-Zn deposit,Sichan. *Journal of KunMing Universtiy of Science and Technology*, 24: 87–94 (in Chinese with English abstract).

Guo Xin, 2011. *Mineralization and metallogenic pattern of lead-zinc deposits in northeast Yunnan*. Beijing: China University of Geosciences (Beijing) (Ph.D thesis): 1–157.

Gemmell, J.B., Sharpe, R., Jonasson, I.R., and Herzig, P.M., 2004. Sulfur isotope evidence for magmatic contributions to submarine and subaerial gold mineralization: conical seamount and the Ladolam gold deposit, Papua New Guinea. *Economic Geology*, 99: 1711–1725.

Han Runsheng, Liu Congqiang, Huang Zhilong, Chen Jin, Ma Deyun, Lei Li and Ma Gengsheng, 2007. Geological features and origin of the Huize carbonate-hosted Zn-Pb-(Ag) District, Yunnan, South China. *Ore Geology Reviews*, 31: 360–383.

Heyl, A.V., Landis, G.P., and Zartman, R.E., 1974. Isotopic Evidence for the Origin of Mississippi Valley-Type Mineral Deposits: A Review. *Economic Geology*, 69: 992–1006.

Holland, H.D., 1965. Some applications of thermochemical data to problems of ore deposits; [Part] 2, Mineral assemblages and the composition of ore forming fluids. *Economic Geology*, 60: 1101–1166.

Hu Ruizhong, Tao Yan, Zhong Hong, Huang Zhilong and Zhang Zhengwei, 2005. Mineralization systems of a mantle plume : A case study from the Emeishan igneous province , southwest China. *Earth Science Frontiers*, 12: 042–054 (in Chinese with English abstract).

Huang Zhilong, Li Xiaobiao, Zhou Meifu, Li Wenbo and Jin Zhongguo, 2010. REE and C-O Isotopic Geochemistry of Calcites from the World-class Huize Pb-Zn Deposits, Yunnan, China: Implications for the Ore Genesis. *Acta Geologica Sinica* (English Edition), 84: 597–613.

Huang Zhilong, Li Wenbo, Chen Jin, Han Runsheng, Liu Congqiang, Xu Cheng and Guan Tao, 2003. Carbon and oxygen isotope constraints on mantle fluidinvolvement in the mineralization of the Huize super-large Pb-Zn deposits, Yunnan Province, China. *Journal of Geochemical Exploration*, 78–79: 637–642.

Huppert, H.E., and Sparks, R.S.J., 1988. The generation of granitic magmas by intrusion of basalt into continental-crust. *Journal of Petrology*, 29: 599–624.

Jørgensen, B.B., Isaksen, M.F., and Jannasch, H.W., 1992. Bacterial Sulfate Reduction Above 100° C in Deep-Sea Hydrothermal Vent Sediments. *Science*, 258: 1756–1757.

Kaiho, K., Kajiwara, Y., Nakano, T., Miura, Y., Kawahata, H., Tazaki, K., Ueshima, M., Chen, Z., and Shi, G.R., 2001. End-Permian catastrophe by a bolide impact: Evidence of a gigantic release of sulfur from the mantle. *Geology*, 29: 815–818.

Kiyosu, Y., and Krouse, H.R., 1990. The role of organic acid in the abiogentic reduction of sulfate and the sulfur isotope effect. *Geochem. J.*, 24: 21–27.

Li Wenbo, Huang Zhilong and Yin Mudan, 2007. Dating of the giant Huize Zn-Pb ore field of Yunnan Province, Southwest China: Constraints from the Sm-Nd system in hydrothermal calcite. *Resource Geology*, 57: 90–97.

Li Xiaobiao, Huang Zhilong, Li Wenbo, Zhang Zhenliang and Yan Zaifei, 2006. Sulfur isotopic compositions of the Huize super-large Pb–Zn deposit, Yunnan Province, China: Implications for the source of sulfur in the ore-forming fluids. *Journal of Geochemical Exploration*, 89: 227–230.

Liu Congqiang, Huang Zhilong, Li Heping and Su Genli, 2001. The geofluid in the mantle and its role in ore-forming processes. *Earth Science Frontiers*, 8: 231–243 (in Chinese with English abstract).

Liu Hechang and Lin Wenda, 1999. *Regularity research of Pb-Zn-Ag ore deposits in north-east Yunnan Province, China*. Kunming: Yunnan University Press (in Chinese).

Liu Wenzhou, 1989. Geological characteristics and genesis of the Jinshachang lead-zinc deposit in Yunnan Province, China. *Journal of Chengdu College of Geology*, 16: 11–19 (in Chinese).

Liu Yun and Bao Huiming, 2009. Oxygen and sulfur isotopic fractionation of sulfate radical between gypsum and aqueous solution. *Acta Mineralogica Sinica*, S1: 285 (in English with Chinese title).

Lombardi, G., and Sheppard, S.M.F., 1977. Petrographic and isotopic studies of the altered acid volcanics of the Tolfa-Cerite area, Italy; the genesis of the clays. *Clay Minerals*, 12: 147–162.

Ma Yansheng, Tao Yan, Zhu Feilin and Wang Xingzhen, 2009. The sulfur isotopic characteristics and geological Significance of Jian Baoshan Pt-Pd deposit and lime nickel deposit. *Bulletin of Mineralogy,Petrology and Geochemistry*, 28: 123–127 (in Chinese with English abstract).

Machel, H., 1989. Relationships between sulphate reduction and oxidation of organic compounds to carbonate diagenesis, hydrocarbon accumulations, salt domes, and metal sulphide deposits. *Carbonates and Evaporites*, 4: 137–151.

Machel, H.G., Krouse, H.R., and Sassen, R., 1995. Products and distinguishing criteria of bacterial and thermochemical sulfate reduction. *Applied Geochemistry*, 10: 373–389.

Mitchell, K., Heyer, A., Canfield, D.E., Hoek, J., and Habicht, K.S., 2009. Temperature effect on the sulfur isotope fractionation during sulfate reduction by two strains of the hyperthermophilic Archaeoglobus fulgidus. *Environmental Microbiology*, 11: 2998–3006.

Ohmoto, H., 1972. Systematics of sulfur and carbon isotopes in hydrothermal ore deposits. *Economic Geology*, 67: 551–578.

Ohmoto, H., and Lasaga, A.C., 1982. Kinetics of reactions between aqueous sulfates and sulfides in hydrothermal systems. *Geochim. Cosmochim. Acta*, 46: 1727–1745.

Peevler, J., Fayek, M., Misra, K.C., and Riciputi, L.R., 2003. Sulfur isotope microanalysis of sphalerite by SIMS: Constraints on the genesis of Mississippi valley-type mineralization, from the Mascot-Jefferson City district, East Tennessee. *Journal of Geochemical Exploration*, 80: 277–296.

Richardson, C.K., Rye, R.O., and Wasserman, M.D., 1988. The chemical and thermal evolution of the fluids in the cave-in-rock fluorspar district, Illinois; stable isotope systematics at the Deardorff Mine. *Economic Geology*, 83: 765–783.

Rye, R.O., 1993. The evolution of magmatic fluids in the epithermal environment; the stable isotope perspective. *Economic Geology*, 88: 733–752.

Rye, R.O., Bethke, P.M., and Wasserman, M.D., 1992. The stable isotope geochemistry of acid sulfate alteration. *Economic Geology*, 87: 225–262.

Rye, R.O., and Ohmoto, H., 1974. Sulfur and carbon isotopes and ore genesis: A Review. *Economic Geology*, 69: 826–842.

Seal, R.R., 2006. Sulfur isotope geochemistry of sulfide minerals. *Reviews in Mineralogy and Geochemistry*, 61: 633–677.

Shields, G.A., Strauss, H., Howe, S.S., and Siegmund, H., 1999. Sulphur isotope compositions of sedimentary phosphorites from the basal Cambrian of China: implications for Neoproterozoic-Cambrian biogeochemical cycling. *Journal of the Geological Society* 156: 943–955.

Sim, M.S., and Bosak, T., Ono, S., 2011. Large sulfur isotope fractionation does not require disproportionation. *Science*, 333: 74–77.

Thode, H.G., and Monster, J., 1967. *Sulfur-isotope geochemistry of petroleum, evaporites, and ancient seas*. Fluids in Subsurfaces Environments: A Symposium, Memoir No. 4. American Association of Petroleum Geologists, 1965; Other Information: Orig. Receipt Date: 31-DEC-67; Bib. Info. Source: DIX (Henry Dix), Medium: X. 367–77.

Tu Guangchi, 1984. *Geochemistry of strata-bound ore deposits in China* (Volumes I). Beijing: Science Press, 38–39 (in Chinese with English abstract).

Wang Xiaochun, Zhang Zheru, Zheng Minghua and Xu Xinhuang, 2000. Metallogenic mechanism of the Tianbaoshan Pb-Zn deposit, Sichuan. *Chinese Journal of Geochemistry*, 19: 121–133.

Yunnan Bureau of Geology, 1978. *Regional geological report: Zhaotong part*. 106 (in Chinese).

Zhang Lisheng, 1997. Hydrothermal karst genesis of stratabound Pb-Zn-(F-Ba) deposits in northeast Yunnan *Acta Geoscientia Sinca*, 18: 41–52 (in Chinese with English abstract).

Zhang Yunxiang, Luo Yaonan and Yang Chongxi, 1988. *Panxi rift*. Beijing: Beijing Geological Press (in Chinese).

Zhou Jiaxi, Huang Zhilong, Zhou Guofa, Li Xiaobiao, Ding Wei and Bao Guangping, 2010. Sulfur isotopic composition of the Tianqiao Pb-Zn ore deposit, Northwest Guizhou Province, China: Implications for the source of sulfur in the ore-forming fluids. *Chinese Journal of Geochemistry*, 29: 301–306.

Zhou, M.-F., Malpas, J., Song, X.-Y., Robinson, P.T., Sun, M., Kennedy, A.K., Lesher, C.M., and Keays, R.R., 2002. A temporal link between the Emeishan large igneous province (SW China) and the end-Guadalupian mass extinction. *Earth and Planetary Science Letters*, 196: 113–122.